Journal Name

Dynamic Article Links ►

Cite this: DOI: 10.1039/c0xx00000x

www.rsc.org/xxxxxx

ARTICLE TYPE

Toward the Creation of Stable, Functionalized Metal Clusters

Yuichi Negishi,*[a] Wataru Kurashige,[a] Yoshiki Niihori[a] and Katsuyuki Nobusada[b]

Received (in XXX, XXX) Xth XXXXXXXXX 20XX, Accepted Xth XXXXXXXXX 20XX
DOI: 10.1039/b000000x

Nanomaterials which exhibit both stability and functionality are currently considered to hold the most promise as components of nanotechnology devices. Thiolate (RS)-protected gold nanoclusters ($Au_n(SR)_m$) have attracted significant attention in this regard and, among these, the magic clusters are believed to be the best candidates since they are the most stable. We have investigated the effects of heteroatom doping, protection by selenolate ligands and protection by photoresponsive thiolates on the stability and physical/chemical properties of these clusters. Through such studies, we have attempted to establish methods of modifying magic $Au_n(SR)_m$ clusters as a means of creating metal clusters that are both robust and functional. This paper summarizes our studies towards this goal and the obtained results.

1. Introduction

Nanomaterials that exhibit both stability and functionality are currently considered to hold the most promise as components of nanotechnology devices. Metal clusters, composed of several to hundreds of metal atoms, possess size-specific physical and chemical properties which are not typically observed in bulk metals, and these properties vary considerably depending on the number of constituent atoms.[1] Metal clusters are therefore attracting significant attention as potentially useful nanomaterials.

The synthesis of metal clusters in this size range incorporating phosphine ligands has been extensively researched since the 1960s. Mingos, Teo, Pignolet, Schmid and Konishi *et al*. have all conducted in-depth research in this field, and their work has resulted in the synthesis of many monometal and alloy clusters.[2–15] The study of these synthesized clusters has provided much important information concerning the stability, structure and physical properties of phosphine-protected metal clusters with ultra-small metal cores. However, since these metal clusters are easily degraded in solution, their poor stability raises questions with regard to their viability as practical materials.[16]

Thiolate-protected gold clusters ($Au_n(SR)_m$), however, as reported in 1994 by Brust *et al*.,[17] exhibit higher stability, due to the strong bonds formed between the metal and the thiolate ligands. These clusters are stable even at high temperature in solution. Hence, since this first report, $Au_n(SR)_m$ clusters have been widely studied by groups representing a variety of fields, and continue to be actively researched.[18–43] The early research of Whetten, Murray and Tsukuda *et al*. provided significant impetus for all such future studies. Their work concerning the precise synthesis of these clusters resulted in several high-resolution separation techniques and precise methods of chemical compositional analysis, and made it possible to treat $Au_n(SR)_m$ clusters as compounds with well-defined chemical compositions. Furthermore, from experiments concerning the stability of a series of clusters, they succeeded in finding specific stable clusters, which were defined as so-called magic clusters.[44–55] Following several misassignments, the chemical compositions of the magic $Au_n(SR)_m$ clusters were found to be $Au_{25}(SR)_{18}$, $Au_{38}(SR)_{24}$ and $Au_{144}(SR)_{60}$.[19,22,51,56,57] More recently, Jin and Dass *et al*. reported that numerous other magic clusters exist[31,58–66] and that magic clusters can be synthesized size-selectively with precision at the atomic level. Among those magic clusters, $Au_{25}(SC_2H_4Ph)_{18}$, $Au_{36}(SPh\text{-}tBu)_{24}$ (SPh-*t*Bu = *4*-tert-butylbenzenethiolate), $Au_{38}(SC_2H_4Ph)_{24}$ and $Au_{102}(p\text{-MBA})_{44}$ (*p*-MBA = *p*-mercaptobenzoic acid) (Figure 1) were successfully

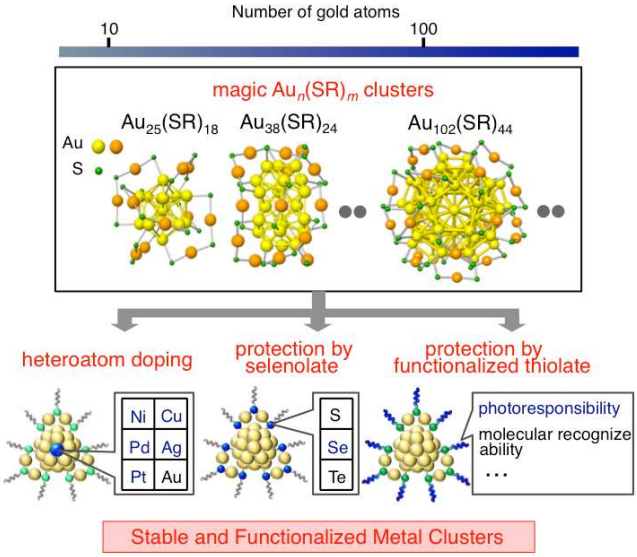

Fig. 1 Our study towards the creation of stable, functionalized metal clusters. In the geometrical structures of $Au_{25}(SR)_{18}$ (Refs. 67 and 68), $Au_{38}(SR)_{24}$ (Ref. 70) and $Au_{102}(SR)_{44}$ (Ref. 31), R groups are omitted for simplicity.

crystalized and their geometrical structures were elucidated experimentally by Kornbeng, Murray, and Jin *et al*.[31,60,67–70] The origins of the stability and electronic states of these compounds were also elucidated, on the basis of theoretical studies, by Hakkinen, Aikens, and Jiang *et al*.[71–74] These experimental and theoretical studies revealed that magic $Au_n(SR)_m$ clusters have a highly symmetrical metal core and are specifically stabilized by such a metal core being protected by multiple gold-thiolate oligomers (−SR−[Au−SR−]$_n$) (Figure 1). The total number of valence electrons associated with the metal cores of these structures is consistent with a closed-shell structure, which also promotes the high stability of these clusters. Many investigations concerning the physical and chemical properties of $Au_n(SR)_m$ clusters have been conducted, and it has been shown that the smaller magic clusters exhibit size-specific physical/chemical properties which are not seen in bulk materials, such as photoluminescence,[19,23,50,51,75–77] optical activity[19,23,33,78] and catalytic activity.[79–82] Furthermore, it has been demonstrated that the surface ligands of these clusters can be exchanged with other ligands (via a ligand exchange reaction) while maintaining the core size,[32,48,49,83–89] making it possible to tune the solubility and electronic structure of the clusters. In this manner, magic $Au_n(SR)_m$ clusters are extremely stable and can be synthesized size-selectively, and yet exhibit size-specific physical and chemical properties, which endows them with great potential as new nanomaterials..

Our group has attempted to establish methods of modifying magic $Au_n(SR)_m$ clusters, with the goal of creating nanomaterials which are both robust and functional, by increasing the functionality of the clusters. As shown in many previous gas phase studies, doping small metal clusters with heteroatoms has a significant effect on their stability as well as their physical and chemical properties.[90] It was therefore anticipated that the properties of magic $Au_n(SR)_m$ clusters would also be significantly modified by doping with heteroatoms. In addition, protection of magic $Au_n(SR)_m$ clusters by selenolate ligands[91] and functionalized thiolates[92] was considered to be useful approachs. Therefore, we have investigated the effects of heteroatom doping, protection by selenolate ligands and protection by functionalized thiolates on the stability and physical/chemical properties of these clusters. Our studies, therefore, have essentially been aimed at devising methods of tailoring magic $Au_n(SR)_m$ clusters to produce compounds which are stable and exhibit useful properties (Figure 1).

The present paper summarizes our work towards this goal and the results. In Section 2, we report the results of heteroatom doping studies, in which magic $Au_n(SR)_m$ clusters were successfully doped with three metal atoms: Pd, Ag and Cu. Investigation of the resulting doped clusters showed the effects of doping on the stability and electronic structures of the clusters. In Section 3, we discuss clusters protected by selenolates, including results showing that incorporating selenolate ligands makes it possible to produce gold clusters which exhibit superior stability in solution as compared to thiolate-protected gold clusters. Furthermore, our results demonstrate that using selenolate ligands also enables the synthesis of alloy clusters that would be difficult to synthesize using thiolates. In Section 4, we report research into clusters protected by photoresponsive thiolates based on an azobenzene derivative, demonstrating that employing these thiolates make it possible to create a Au_{25} cluster which exhibits reversible changes in redox potential in response to photoirradiation. Finally, in Section 5, we summarize our work and briefly describe potential future research directions in this field.

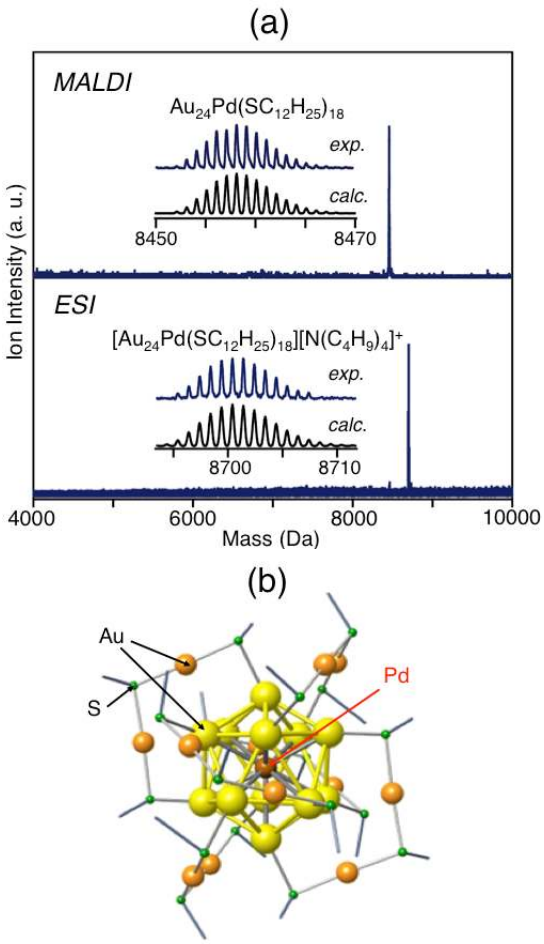

Fig. 2 (a) Negative-ion MALDI and positive−ion electrospray ionization (ESI) mass spectra of $[Au_{24}Pd(SC_{12}H_{25})_{18}]^0$. Insets compare experimental data with the calculated isotope patterns. In the ESI mass analysis, a small amount of $(C_4H_9)_4NClO_4$ was added to the solution to allow observation of neutral $[Au_{24}Pd(SC_{12}H_{25})_{18}]^0$ as a cation. (b) Optimized structure of $[Au_{24}Pd(SCH_3)_{18}]^0$ (adapted from Refs. 88 and 98).

2. Heteroatom Doping

2.1. Pd doping

2.1.1. $Au_{24}Pd(SR)_{18}$

With regard to Pd doping, several studies have preceded our own. In 2009, Murray *et al*. succeeded in synthesizing a $Au_{24}Pd$ cluster ($Au_{24}Pd(SC_2H_4Ph)_{18}$) using phenylethanethiol (PhC_2H_4SH) as the ligand.[93] Following this report, three groups independently performed density functional theory (DFT) calculations concerning $Au_{24}Pd(SCH_3)_{18}$.[94–96] These analyses resulted in two conclusions regarding this compound; its most stable structure is a core-shell-type $Pd@Au_{24}(SR)_{18}$ formation in which the central Au in $Au_{25}(SR)_{18}$ is replaced by Pd, and replacing the central Au

in this manner increases the interaction energy between the central atom and the $Au_{24}(SCH_3)_{18}$ cage, which in turn increases the thermodynamic stability of the cluster. With the aim of producing clusters which are more stable than $Au_n(SR)_m$, we focused on these theoretical predictions and attempted to isolate $Au_{24}Pd(SR)_{18}$ and elucidate its structure and stability, as well as its chemical properties.

Isolation

In our study, we used dodecanethiol ($C_{12}H_{25}SH$) as the ligand[97] and dodecanethiolate-protected $Au_{24}Pd$ clusters ($Au_{24}Pd(SC_{12}H_{25})_{18}$) were synthesized using the Burst method.[17] In this process, gold and palladium salts were transferred from an aqueous phase to a toluene phase with a phase transfer compound, and $C_{12}H_{25}SH$ was added to the toluene phase. Adding a reducing agent to this solution produced a mixture of $C_{12}H_{25}S$-protected Au-Pd alloy clusters of various sizes. The resulting mixture was subsequently dried after which we separated out only the smallest clusters (those containing 25 metal atoms) based on size-related differences in the solubilities of the clusters (An Acetone was used as the solvent for extraction). Matrix-assisted laser desorption/ionization (MALDI) mass analysis of the product demonstrated that it was composed of $Au_{25}(SC_{12}H_{25})_{18}$ and $Au_{24}Pd(SC_{12}H_{25})_{18}$. We next performed a high resolution separation of these two clusters using high performance liquid chromatography (HPLC) with reverse phase columns. $Au_{25}(SC_{12}H_{25})_{18}$ is usually synthesized in its anionic form as $[Au_{25}(SC_{12}H_{25})_{18}]^-$,[54,67,68] while $Au_{24}Pd(SC_{12}H_{25})_{18}$ is produced as the neutral compound $[Au_{24}Pd(SC_{12}H_{25})_{18}]^0$ (Figure 2(a)).[98] The two can thus be efficiently separated with reverse phase columns due to differences in their charge states. Using this method, we succeeded in isolating $[Au_{24}Pd(SC_{12}H_{25})_{18}]^0$ at an atomic level of precision (Figure 2(a)).[98]

Structure

$[Au_{25}(SR)_{18}]^-$ has been found to have a structure in which a Au_{13} core is surrounded by six $-SR-[Au-SR-]_2$ oligomers (Figure 1).[67,68] Considering that $[Au_{24}Pd(SC_{12}H_{25})_{18}]^0$ has the same number of metal atoms and organic moieties as $[Au_{25}(SR)_{18}]^-$, we would anticipate that the two have similar geometrical structures (Figure 1). It is also known that only a single Pd is doped into $Au_{25}(SC_{12}H_{25})_{18}$, regardless of the experimental conditions,[93,98] and that the Au and Pd readily form a core-shell-type structure.[98] Furthermore, theoretical calculations predict that the most stable structure for $[Au_{24}Pd(CH_3)_{18}]^0$ is a core-shell-type $[Pd@Au_{24}(SR)_{18}]^0$ structure.[95,96] Considering these three factors, it is reasonable to expect that the $[Pd@Au_{24}(SC_{12}H_{25})_{18}]^0$ structure exists (Figure 2(b)), in which the central Au in $Au_{25}(SC_{12}H_{25})_{18}$ is replaced with Pd. To confirm this, the optical absorption spectrum and X-ray diffraction pattern of $[Au_{24}Pd(SCH_3)_{18}]^0$, in which SCH_3 is the ligand, were calculated and compared with the experimental results obtained for $[Pd@Au_{24}(SC_{12}H_{25})_{18}]^0$. This comparison showed very good agreement between the experimental results and the calculated data.[98] On the basis of these results, we conclude that $[Au_{24}Pd(SC_{12}H_{25})_{18}]^0$ does indeed possess a core-shell-type $[Pd@Au_{24}(SC_{12}H_{25})_{18}]^0$ structure, in which the central Au in $Au_{25}(SC_{12}H_{25})_{18}$ is replaced with Pd.

Stability

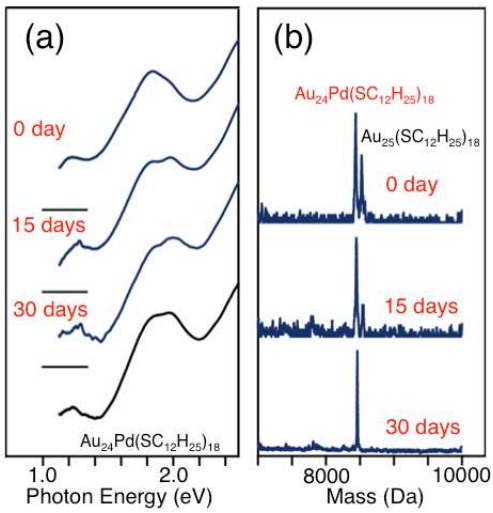

Fig. 3 (a) Time dependence of optical absorption spectra of a toluene solution containing $Au_{25}(SC_{12}H_{25})_{18}$ and $Au_{24}Pd(SC_{12}H_{25})_{18}$ at 50 °C. (b) Chemical composition of the solution as followed by negative−ion MALDI mass spectrometry. After 30 days, the optical absorption spectrum is similar to that of $Au_{24}Pd(SC_{12}H_{25})_{18}$, and the mass spectrum exhibits only the peak attributed to $Au_{24}Pd(SC_{12}H_{25})_{18}$. These results demonstrate that $Au_{24}Pd(SC_{12}H_{25})_{18}$ is more stable in solution than $Au_{25}(SC_{12}H_{25})_{18}$ (adapted from Ref. 98).

DFT calculations predicted that replacing the central Au of $Au_{25}(SR)_{18}$ with Pd would increase the thermodynamic stability of the cluster,[94,95] and our study confirmed that $Au_{24}Pd(SC_{12}H_{25})_{18}$ is actually more resistant to degradation in solution than $Au_{25}(SC_{12}H_{25})_{18}$.[98] To assess stability, we dispersed both $Au_{24}Pd(SC_{12}H_{25})_{18}$ and $Au_{25}(SC_{12}H_{25})_{18}$ in toluene at 50 ºC and examined changes in the chemical composition of the mixture through optical absorption spectroscopy and MALDI mass spectrometry. The optical absorption spectrum of the mixture changed continuously over time, and after 30 days it was very close to that of pure $[Au_{24}Pd(SC_{12}H_{25})_{18}]^0$ (Figure 3(a)), indicating that $Au_{25}(SC_{12}H_{25})_{18}$ deteriorates more rapidly than $Au_{24}Pd(SC_{12}H_{25})_{18}$ under these conditions. In addition, the MALDI mass spectrum of the mixture only exhibited a peak attributed to $Au_{24}Pd(SC_{12}H_{25})_{18}$ after 30 days (Figure 3(b)). Based on these results, it is evident that $Au_{24}Pd(SC_{12}H_{25})_{18}$ is more stable in solution than $Au_{25}(SC_{12}H_{25})_{18}$.

As noted above, DFT calculations predicted that replacing the central Au of $Au_{25}(SR)_{18}$ with Pd would increase the interaction energy between the central atom and the $Au_{24}(SCH_3)_{18}$ cage. Based on this theoretical prediction, the variation in thermodynamic stability between $Au_{24}Pd(SC_{12}H_{25})_{18}$ and $Au_{25}(SC_{12}H_{25})_{18}$ is considered to be due to this difference in interaction energy. The more robust structural skeleton of $Au_{24}Pd(SC_{12}H_{25})_{18}$ therefore is responsible for its superior stability compared to $Au_{25}(SC_{12}H_{25})_{18}$.

Ligand−exchange reactivity

We have demonstrated that Pd doping also significantly increases the ligand-exchange reactivity of $Au_{25}(SC_{12}H_{25})_{18}$.[88] The ligand-exchange reaction replaces a portion (or all) of the cluster's ligands with new ligands. This phenomenon can be used to tailor the solubility of a cluster and to introduce new functional ligands, as demonstrated by several

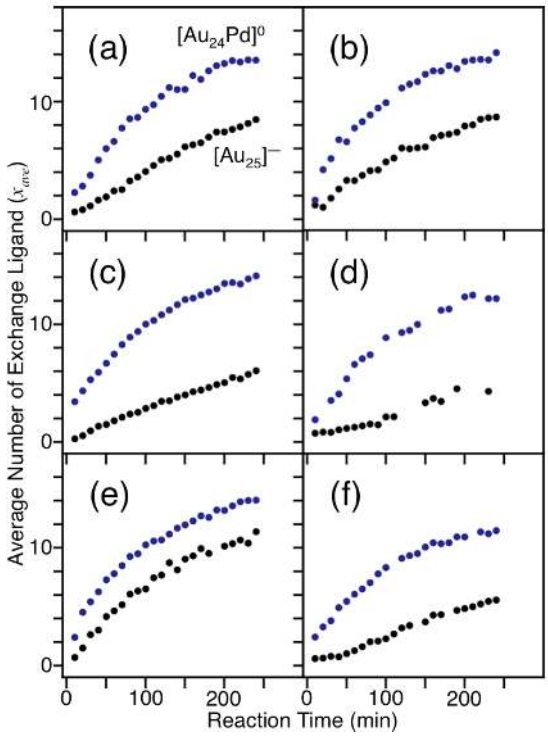

Fig. 4 The results of the ligand−exchange reactions of $[Au_{24}Pd(SC_{12}H_{25})_{18}]^0$ (blue) and $[Au_{25}(SC_{12}H_{25})_{18}]^-$ (black). Plots indicate the average number of exchanged ligands, x_{ave}, against reaction time: (incoming thiol, solvent) = (a) ($C_6H_{13}SH$, CH_2Cl_2); (b) ($C_8H_{17}SH$, CH_2Cl_2); (c) ($C_{10}H_{21}SH$, CH_2Cl_2), (d) ($C_{16}H_{33}SH$, CH_2Cl_2); (e) (PhC_2H_4SH, CH_2Cl_2) and (f) ($C_8H_{17}SH$, toluene) (adapted from Ref. 88). The value of x_{ave} was estimated from the negative−ion MALDI mass spectra of the products.

studies.[32,48,49,83–89] Furthermore, both the redox potential[100,101] and photoluminescence quantum yield[77] of $Au_{25}(SR)_{18}$ vary depending on the ligand. The use of the ligand-exchange reaction can also alter various chemical and physical properties of the cluster and thus is an important means of tuning cluster properties. To assess this effect, we reacted $[Au_{24}Pd(SC_{12}H_{25})_{18}]^0$ and $[Au_{25}(SC_{12}H_{25})_{18}]^-$ with thiols (so-called incoming thiols) in solution and compared the reaction rates in order to investigate the effects of Pd doping on the ligand-exchange reactivity of $Au_{25}(SR)_{18}$. Throughout these trials, the chemical compositions of the products were characterized by MALDI mass spectrometry[49,102] and the average number of exchanged ligands, x_{ave}, at various points in the reaction was estimated from the mass spectra. These experiments were conducted with various incoming thiols and solvents[88] and showed that the x_{ave} value of $[Au_{24}Pd(SC_{12}H_{25})_{18}]^0$ is approximately 1.5–4.2 times greater than that of $[Au_{25}(SC_{12}H_{25})_{18}]^-$ (Figure 4).[88] As noted above, Pd doping increases the resistance of $Au_{25}(SR)_{18}$ to degradation (or unimolecular dissociation[51]) in solution.[88,98] These results indicate that Pd doping actually has two beneficial results; it suppresses unimolecular dissociation of the cluster in solution and also increases ligand-exchange reactivity.

We believe that the increased rate of ligand exchange which follows Pd doping is related to the difference in the total numbers of valence electrons in the metal cores of $[Au_{25}(SC_{12}H_{25})_{18}]^-$ and $[Au_{24}Pd(SC_{12}H_{25})_{18}]^0$. Song and Murray[103] found that the rate of ligand exchange of $Au_{144}(SR)_{60}$ varied depending on the charge state (*i.e.,* the total number of valence electrons) of the metal core such that, when the gold core was oxidized from a neutral state to a charge of +3, the rate of ligand exchange nearly doubled. Our group similarly studied the dependence of the reaction rate on the charge state of $Au_{25}(SC_{12}H_{25})_{18}$ and found that, even in the case of $Au_{25}(SC_{12}H_{25})_{18}$, the reaction rate exhibits a similar dependence on the charge state; when the gold core was oxidized and transitioned from an anionic to a neutral state, similar increases in its reaction rate were observed.[88] We know that the anion $[Au_{25}(SC_{12}H_{25})_{18}]^-$ is the most stable synthesis product whereas, in the case of $Au_{24}Pd(SC_{12}H_{25})_{18}$, the neutral species $[Au_{24}Pd(SC_{12}H_{25})_{18}]^0$ is obtained. The total numbers of valence electrons in these clusters are respectively calculated to be 8 and 6, indicating that $[Au_{24}Pd(SC_{12}H_{25})_{18}]^0$ has two fewer valence electrons than $[Au_{25}(SC_{12}H_{25})_{18}]^-$. This reduction in the number of valence electrons in the cluster, equivalent to a reduced charge density, is likely to promote attack by incoming nucleophilic ligands[103] on the cluster,[32] resulting in an increase in the reaction rate.

Heinecke *et al.*[32] have, however, reported that the ease of ligand exchange in $Au_{102}(p\text{-MBA})_{44}$ (*p*-MBA = *p*-mercaptobenzoic acid) is strongly related to its geometric structure. They determined that those ligands in $Au_{102}(p\text{-MBA})_{44}$ which were more physically accessible to incoming thiols were preferentially exchanged. Our previous study revealed that Pd doping distorts the structure of $[Au_{25}(SC_{12}H_{25})_{18}]^-$ (Ref. 98) and so the dramatic increase in the reaction rate on Pd doping may be partly due to this distortion of the geometric structure, in addition to the above-noted electronic factors.

2.1.2. $Au_{36}Pd_2(SR)_{24}$

Our work therefore showed that doping $Au_{25}(SR)_{18}$ with Pd forms a more stable cluster than the monometallic $Au_{25}(SR)_{18}$. We next wished to determine if this same increased stability on Pd doping would take place with other magic $Au_n(SR)_m$ clusters, and so we isolated high purity $Au_{36}Pd_2(SC_2H_4Ph)_{24}$, in which two Pd atoms are doped into $Au_{38}(SC_2H_4Ph)_{24}$, and examined its stability in solution.

Isolation

In this study, we used phenylethanethiol (PhC_2H_4SH) as the ligand.[97] A mixture of Au−Pd alloy clusters was initially prepared by reacting gold and palladium salts with PhC_2H_4SH in tetrahydrofuran (THF) and reducing the resulting complexes with $NaBH_4$ (upper part of Figure 5(a)).[47,104,105] This preparation process has been reported by Qian *et al.*[106] We then separated $Au_{36}Pd_2(SC_2H_4Ph)_{24}$ from the mixture using the following two steps.

Firstly, the two species $Au_{38-n}Pd_n(SC_2H_4Ph)_{24}$ (n = 1, 2) were separated from the mixture. This step involved initially removing $Au_{25-n}Pd_n(SC_2H_4Ph)_{18}$ (n = 0, 1) from the mixture based on differences in their solubility. $Au_{38-n}Pd_n(SC_2H_4Ph)_{24}$ (n = 1, 2) clusters were then separated from larger clusters using recycling size exclusion chromatography. The MALDI mass spectrum of the product confirmed that only the $Au_{38-n}Pd_n(SC_2H_4Ph)_{24}$ (n = 1,

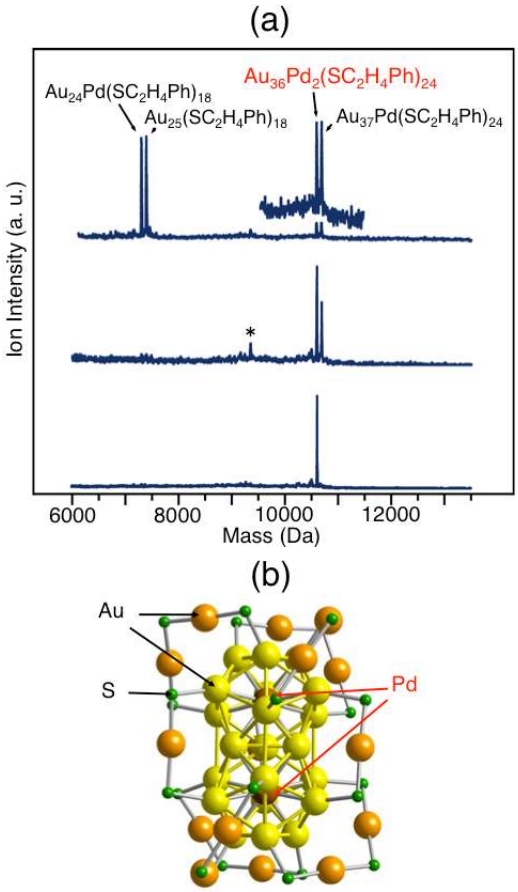

Fig. 5 (a) Negative−ion MALDI mass spectra of (top) as-prepared clusters, (middle) the product separated by recycling size exclusion chromatography and (bottom) after stirring in THF solution at 60 °C for 8 days. The asterisk indicates the laser fragmentation ion of $Au_{37}Pd(SC_2H_4Ph)_{24}$ (See Ref. 105). (b) Optimized structure for $[Au_{36}Pd_2(SCH_3)_{24}]^{2-}$ (the CH_3 moiety is omitted for clarity) (adapted from Ref. 105).

2) clusters were present (central portion of Figure 5(a)).

Next, the $Au_{37}Pd(SC_2H_4Ph)_{24}$ in the product was preferentially decomposed. In this step, the product was stirred for 8 days in THF at 60 °C. The MALDI mass spectrum of the product after 8 days exhibited only a peak attributed to $Au_{36}Pd_2(SC_2H_4Ph)_{24}$ (MW = 10597.0) (lower portion of Figure 5(a)). The product was further characterized by various techniques, including electrospray ionization (ESI) mass spectrometry and thermogravimetric analysis. The results demonstrated that the product had a chemical composition matching $Au_{36}Pd_2(SC_2H_4Ph)_{24}$, and thus this material had been successfully isolated in high purity using this experimental method.[105]

Structure

Isolated $Au_{36}Pd_2(SC_2H_4Ph)_{24}$ is expected to have a similar geometric structure to $Au_{38}(SC_2H_4Ph)_{24}$, since they both have the same number of metal atoms and ligands. $Au_{38}(SC_2H_4Ph)_{24}$ has a structure in which multiple Au(I)-SC_2H_4Ph oligomers cover a Au_{23} core, which consists of two linked icosahedral Au_{13} groups (Figure 1).[70] Our studies on $Au_{24}Pd(SR)_{18}$ have shown that substitution of Pd for Au occurs in the center of the Au_{13} core (**2.1.1**)[98] and therefore it follows that $Au_{36}Pd_2(SC_2H_4Ph)_{24}$ also

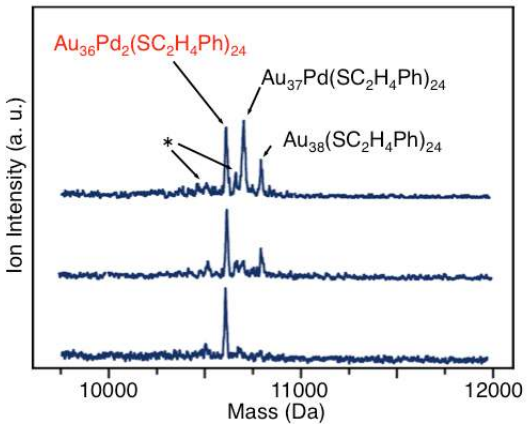

Fig. 6 Time−dependent negative−ion MALDI mass spectra of a THF solution containing $Pd_2Au_{36}(SC_2H_4Ph)_{24}$, $PdAu_{37}(SC_2H_4Ph)_{24}$ and $Au_{38}(SC_2H_4Ph)_{24}$ at 60 °C. The asterisk indicates the laser fragmentation ions of $Au_{38}(SC_2H_4Ph)_{24}$ (See Ref. 105) (adapted from Ref. 105).

assumes a structure with a $Au_{21}Pd_2$ core, where two Au atoms in the center of the Au_{13} are replaced with Pd atoms, and in which the core is covered by multiple Au(I)-SC_2H_4Ph oligomers (Figure 5(b)). DFT calculations concerning $Au_{36}Pd_2(SCH_3)_{24}$ have demonstrated that the structure represented in Figure 5(b) is in fact energetically stable.[107]

Stability

Stability experiments revealed that $Au_{36}Pd_2(SC_2H_4Ph)_{24}$ also exhibits higher resistance to degradation in solution than does $Au_{38}(SC_2H_4Ph)_{24}$. In these trials, a THF solution containing $Au_{36}Pd_2(SC_2H_4Ph)_{24}$, $Au_{37}Pd(SC_2H_4Ph)_2$ and $Au_{38}(SC_2H_4Ph)_{24}$ was continually stirred at 60 ºC. MALDI mass analysis of the mixture at various intervals revealed that $Au_{38}(SC_2H_4Ph)_{24}$ deteriorated more quickly than $Au_{36}Pd_2(SC_2H_4Ph)_{24}$ (Figure 6),[105] indicating that the doping of $Au_{38}(SC_2H_4Ph)_{24}$ with two Pd atoms forms a cluster that is more stable against degradation in solution than the monometallic $Au_{38}(SC_2H_4Ph)_{24}$. Similar results were also obtained when assessing stability against core etching by thiols.[105] As noted, DFT studies found that, when an Au atom in the center of the Au_{13} core in $Au_{25}(SR)_{18}$ is replaced by a Pd atom, the interaction energy between the central atom and the surrounding cage structure increases.[94] The same manner of increase in interaction energy occurs when Pd atoms are doped, even in $Au_{38}(SC_2H_4Ph)_{24}$, which explains the increased resistance of $Au_{36}Pd_2(SC_2H_4Ph)_{24}$ to both degradation in solution and core etching by thiols compared to $Au_{38}(SC_2H_4Ph)_{24}$.

In contrast, $Au_{37}Pd(SC_2H_4Ph)_{24}$, which is doped with a single Pd atom, decomposes more quickly in both THF and in neat PhC_2H_4SH than $Au_{38}(SC_2H_4Ph)_{24}$ (Figure 6).[105] It is expected that replacing a Au atom in the center of the Au_{13} core by a Pd atom increases the interaction energy between the central atom and the surrounding cage structure. However, doping with a single Pd atom also decreases the symmetry of the structure, and we consider that the associated decrease in the stability of the cluster leads to more rapid decomposition of $Au_{37}Pd(SC_2H_4Ph)_{24}$ as compared to the monometallic $Au_{38}(SC_2H_4Ph)_{24}$.

2.2. Ag doping

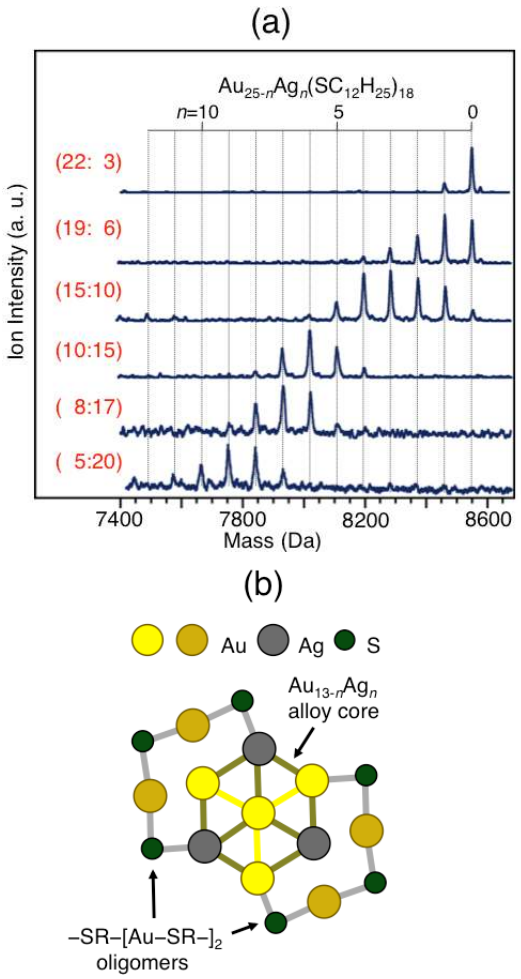

Fig. 7 (a) Negative−ion MALDI mass spectra of $Au_{25-n}Ag_n(SC_{12}H_{25})_{18}$ synthesized at varying Au:Ag ratios. Ratios represent the relative reactant proportions $[HAuCl_4]$:$[AgNO_3]$. (b) Proposed structure for $Au_{25-n}Ag_n(SC_{12}H_{25})_{18}$ (n = 0−12) (adapted from Ref. 108).

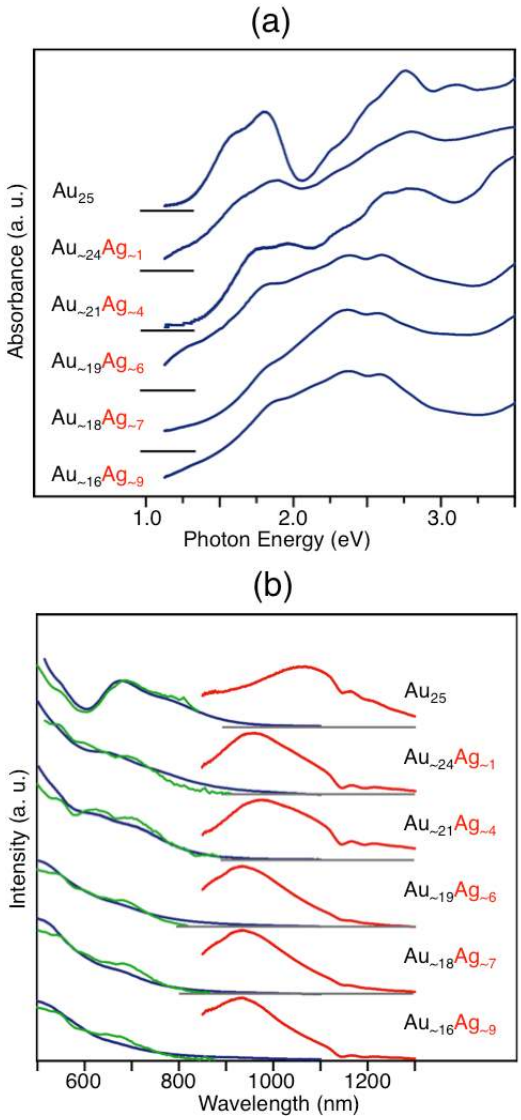

Fig. 8 (a) Optical absorption spectra and (b) optical absorption (blue), photoemission (red) and photoexcitation (green) spectra of toluene solutions of $Au_{25-n}Ag_n(SC_{12}H_{25})_{18}$ (n = 0−12). Photoemission spectra were obtained using excitation at 570 nm (adapted from Ref. 108).

2.2.1. $Au_{25-n}Ag_n(SR)_{18}$

The element Ag (1.44 Å) is similar to Au (1.44 Å) in many ways, since both have a single valence electron and virtually the same atomic radius. It should therefore be possible to dope several Ag atoms into magic $Au_n(SR)_m$ clusters more readily than when working with Pd. The electronic structures and physical properties of the resulting doped clusters were expected to continuously vary with increasing levels of Ag doping and this expectation prompted us to study the Ag doping of $Au_{25}(SR)_{18}$.

Synthesis

In this work, we used $C_{12}H_{25}SH$ as the ligand.[97] $Au_{25-n}Ag_n(SC_{12}H_{25})_{18}$ was synthesized using a method similar to that used to make $Au_{24}Pd(SC_{12}H_{25})_{18}$ (see Section **2.1**).[98] MALDI mass analysis of the product demonstrated that a number of Ag-doped $Au_{25-n}Ag_n(SC_{12}H_{25})_{18}$ clusters were synthesized by this method and the number of the Ag atoms included in the clusters increased continuously with the molar ratio of silver to gold salts applied during synthesis (Figure 7(a)).[108] The quantity of added Ag atoms increased to n = 12 when the [gold salt]:[silver salt] ratio was 5:20 (Figure 7(a)).[108] As noted, the atomic radii of Ag (1.44 Å) and Au (1.44 Å) are virtually identical, and both elements possess a single s valence electron. It follows that the Au atoms should be readily replaced with Ag, leading to the formation of $Au_{25-n}Ag_n(SC_{12}H_{25})_{18}$ clusters in which multiple Au atoms are replaced by Ag atoms. Jin *et al*. has also succeeded in synthesizing $Au_{25-n}Ag_n(SR)_{18}$.[109]

Structure

It is reasonable to assume, from its chemical composition, that $Au_{25-n}Ag_n(SC_{12}H_{25})_{18}$ has the same skeletal structure as $Au_{25}(SR)_{18}$. Several groups have performed theoretical calculations to elucidate the positions of the Ag dopant atoms in these alloy clusters. Walter *et al*. performed DFT calculations for $[Au_{24}Ag(SCH_3)_{18}]^x$ ($-1 \le x \le +1$) and reported that the structure in which Ag is located at the surface of the Au_{13} core is the most energetically stable.[96] Aikens *et al*. performed DFT calculations for $[Au_{25-n}Ag_n(SH)_{18}]^-$ ($n \le 12$) doped with multiple Ag atoms, and determined that, regardless of the number of dopant atoms,

the structures in which Ag is found at the surface of the Au_{13} core are the most energetically stable.[110] The same findings were reported by Kauffman *et al.* based on DFT calculations concerning $[Au_{22}Ag_3(SH)_{18}]^-$.[111] On the basis of these results, Ag is expected to be preferentially positioned at the surface of the metal core in $Au_{25-n}Ag_n(SC_{12}H_{25})_{18}$. That is, $Au_{25-n}Ag_n(SC_{12}H_{25})_{18}$ (n = 0–12) should have a structure in which a $Au_{13-n}Ag_n$ alloy core is surrounded by six −SR−[Au−SR−]$_2$ oligomers, where R is $C_{12}H_{25}$ (Figure 7(b)). The $Au_{25-n}Ag_n(SC_{12}H_{25})_{18}$ (n = 0–12) clusters should therefore be stable since stable −SR−[Au−SR−]$_2$ oligomers are formed on their surfaces, just as they are in $Au_{25}(SR)_{18}$. We did find, however, that, irrespective of the synthesis conditions, $Au_{25-n}Ag_n(SC_{12}H_{25})_{18}$ clusters containing more than 14 Ag atoms are not produced.[108] We believe these clusters are unstable because the larger proportion of Ag leads to incorporation of Ag atoms into the oligomers, and thus the metal core is no longer surrounded solely by stable −SR−[Au−SR−]$_2$ oligomers.

Electronic structures

Optical absorption spectroscopy of $Au_{25-n}Ag_n(SC_{12}H_{25})_{18}$ (n = 0–12) revealed that the electronic structures of these clusters could be continuously varied by increasing the extent of Ag doping.[108] The $Au_{25}(SC_{12}H_{25})_{18}$ spectrum exhibits a characteristic peak in the region 1.5–2.0 eV (Figure 8(a)), attributed to the highest occupied molecular orbital (HOMO: the occupied Au 6sp orbital in the Au_{13} core) to lowest unoccupied molecular orbital (LUMO: the unoccupied Au 6sp orbital in the Au_{13} core) transition, based on DFT calculations concerning $Au_{25}(SCH_3)_{18}$.[68,71,112,113] Increased Ag doping shifts this peak to higher energy levels,[108] indicating an associated steady increase in the HOMO–LUMO gap of the cluster. The photoluminescence emission of the clusters also gradually shifts to shorter wavelengths with increasing levels of Ag doping (Figure 8(b)).[108] Kauffman *et al.* performed electrochemical measurements on $Au_{\sim 22}Ag_{\sim 3}(SC_2H_4Ph)_{18}$ and reported that, because Ag doping raises the orbital energy of the cluster's LUMO, the HOMO−LUMO gap is increased.[111] All these results indicate that Ag doping is an effective means of creating stable clusters with larger HOMO−LUMO gaps than the original magic $Au_{25}(SR)_{18}$.

2.2.2 $Au_{38-n}Ag_n(SR)_{24}$ and $Au_{144-n}Ag_n(SR)_{60}$

Regarding the larger Ag-doped clusters, Dass *et al.* have successfully synthesized larger Ag-doped magic $Au_n(SR)_m$ clusters, with up to 12 Ag atoms in $Au_{38}(SC_2H_4Ph)_{24}$ and up to 60 in $Au_{144}(SC_2H_4Ph)_{60}$.[114,115] On the basis of various findings, they pointed out that the majority of Ag atoms are doped at the surface of the metal cores of these clusters although a part of Ag atoms may be doped in the oligomers of these clusters.[114,115] Häkkinen *et al.* studied the geometrical structure of $Au_{144-n}Ag_n(SR)_{60}$ using DFT calculations, and reported that the structure in which Ag is doped into the surface of the metal core is the most energetically stable.[116] In addition, Dass *et al.* investigated the effect of Ag doping on the optical absorption spectrum, and determined that, while the peak structure is continuously eroded with increasing doping number in the case of $Au_{38}(SR)_{24}$,[114] two plasmon-like peaks continuously increase with increasing doping number when working with $Au_{144}(SR)_{60}$.[115]

2.3. Cu doping

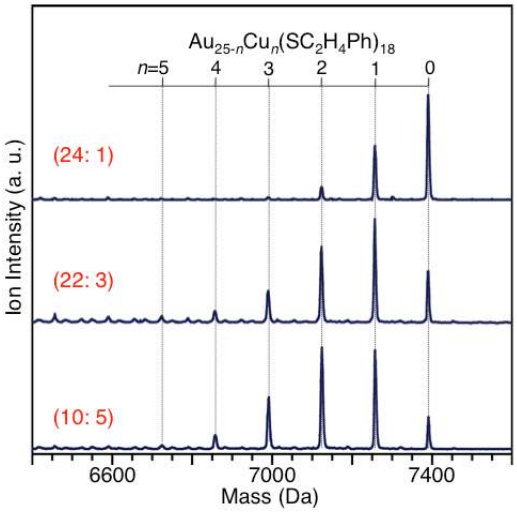

Fig. 9 Negative−ion MALDI mass spectra of $Au_{25-n}Cu_n(SC_2H_4Ph)_{18}$ synthesized at varying Au:Cu ratios. Ratios represent the relative reactant proportions $[HAuCl_4]$:$[CuCl_2]$ (adapted from Ref. 117).

Copper is also in the same family as Au and so it seems reasonable to expect to add several Cu atoms into the magic $Au_n(SR)_m$ clusters, such that the electronic structures and physical properties of the clusters are continuously varied by increasing the level of Cu doping. Cu is different from Ag, however, in that its atomic radius (1.28 Å) is smaller than that of Au (1.44 Å) and the Au–Cu bond is stronger than the Au–Au bond. We investigated how doping with such an element affects the structure and stability of $Au_{25}(SR)_{18}$.

Synthesis

$Au_{25-n}Cu_n(SR)_{18}$ was synthesized via a similar method to that used to make $Au_{24}Pd(SR)_{18}$ (see Section **2.1**) and $Au_{25-n}Ag_n(SR)_{18}$.[97] Mass spectrometry of the product demonstrated that Cu-doped $Au_{25-n}Cu_n(SR)_{18}$ had been synthesized using this technique (Figure 9).[117] However, in contrast to the case of $Au_{25-n}Ag_n(SR)_{18}$,[108] $Au_{25-n}Cu_n(SC_2H_4Ph)_{18}$ clusters with many copper atoms ($n \geq 6$) were rarely obtained, regardless of the experimental conditions (Figure 9).[117] As Cu has a smaller atomic radius than Au, Cu doping significantly distorts the cluster structure, causing the cluster to become unstable at higher doping levels.[117] Consequently, only up to five copper atoms can be doped into $Au_{25}(SR)_{18}$, significantly lower than the extent of Ag doping which can be achieved.

Structure

Given the chemical composition of $Au_{25-n}Cu_n(SR)_{18}$, we can assume that $Au_{25-n}Cu_n(SR)_{18}$ also has a skeletal structure similar to that of $Au_{25}(SR)_{18}$. To the best of our knowledge, there were no reports on the positions of Cu dopant atoms in $Au_{25-n}Cu_n(SR)_{18}$ and so we carried out studies to elucidate the doping positions, from both theoretical and experimental viewpoints, although the results do not allow any definitive conclusions. The optimum structures of the cluster doped at each potential doping site (the center of the Au_{13} core, the surface of the Au_{13} core and the −SR−[Au−SR−]$_2$ oligomers) indicate that the geometric structure of the cluster is significantly distorted when copper is inserted at any of these locations.[117] These results differ from

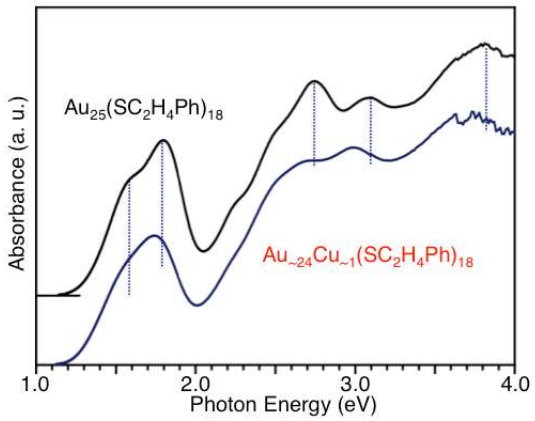

Fig. 10 Optical absorption spectra of $Au_{\sim24}Cu_{\sim1}(SC_2H_4Ph)_{18}$ and $[Au_{25}(SC_2H_4Ph)_{18}]^-$. Dotted lines indicate the main peak positions in the absorption spectrum of $[Au_{25}(SC_2H_4Ph)_{18}]^-$ (adapted from Ref. 117).

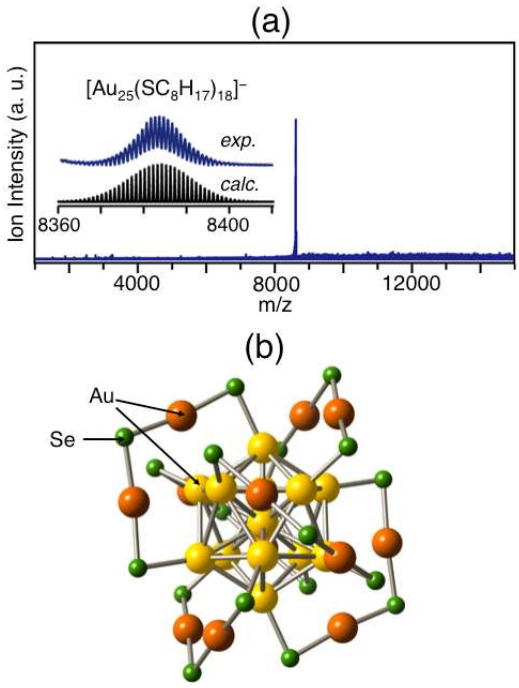

Fig. 11 (a) Negative−ion ESI mass spectra of $[Au_{25}(SC_8H_{17})_{18}]^-$. Inset compares experimental data with the calculated isotope pattern. (b) Optimized structure of $[Au_{25}(SCH_3)_{18}]^-$ (the CH_3 moiety is omitted for clarity) (adapted from Refs. 127 and 128).

those for silver doping, where our own DFT calculations[117] and those by Aikens *et al*.[110] imply that silver doping produces only minimal structural distortion, regardless of the doping site. Because copper doping significantly distorts the cluster structure, the number of doped atoms is considered to be limited to a relatively low value (~5) for $Au_{25-n}Cu_n(SC_2H_4Ph)_{18}$ (Figure 9).

Electronic structures

Optical absorption spectroscopy of $Au_{25-n}Cu_n(SC_2H_4Ph)_{18}$ revealed that, in contrast to the case of Ag doping, Cu doping reduces the cluster's HOMO−LUMO gap (Figure 10).[117] Electrochemical measurements of $Au_{25-n}Cu_n(SC_2H_4Ph)_{18}$ also indicated that Cu doping lowers the orbital energy of the cluster's LUMO,[117] leading to a decrease in the HOMO−LUMO gap. As noted, when thiolate is used as the ligand, as many as five Cu atoms can be doped into the Au_{25} cluster. However, as will be described later (Section **3.2**), when selenolate is used as the ligand up to nine Cu atoms may be added into the Au_{25} cluster. Furthermore, the number of Cu atoms inserted can be varied continuously depending on the preparative conditions.[118] Optical absorption, differential pulse voltammetry and photoluminescence measurements of the series of $Au_{25-n}Cu_n(SeR)_{18}$ (n = 1−9) clusters revealed that Cu doping continuously reduces the HOMO−LUMO gap and continuously shifts the emission wavelength to longer wavelengths (Section **3.2**).[118] These results demonstrate that Cu doping is an effective means for creating clusters with smaller HOMO−LUMO gaps than magic $Au_{25}(SR)_{18}$.

Stability

Cu doping was found to significantly reduce the stability of the clusters in solution.[117] Jin *et al*. reported similar results, which showed the instability of $Au_{25-n}Cu_n(SC_2H_4Ph)_{18}$.[109] Despite the bond between Au and Cu being stronger than that between Au and Au, the stability of $Au_{25-n}Cu_n(SR)_{18}$ is less than that of $Au_{25}(SR)_{18}$, which may be attributed to the induced strain in the Cu-doped cluster due to the size mismatch between Cu and Au. Such significant reduction in stability was not observed upon silver doping, suggesting that the geometric structure strongly affects the stability of $[Au_{25}(SR)_{18}]^-$. Thus, it is necessary to select a doping element which has a very similar atomic radius to that of gold in order to functionalize $[Au_{25}(SR)_{18}]^-$ while maintaining its stability.

2.4. Doping with other metals

Recently, doping with heteroatoms has been studied by many groups and several reports have appeared concerning doping elements other than those discussed above. Jin *et al*. have reported the synthesis of $Au_{24}Pt(SR)_{18}$, which was produced by doping $Au_{25}(SR)_{18}$ with Pt.[119] On the basis of various structural analyses, they concluded that, as was the case with $Au_{24}Pd(SR)_{18}$, $Au_{24}Pt(SR)_{18}$ has a core-shell-type $Pt@Au_{24}(SR)_{18}$ structure.[119,120] The $Pt@Au_{24}(SR)_{18}$ thus synthesized was isolated as the neutral species $[Au_{24}Pt(SR)_{18}]^0$, and the total number of valence electrons in the metal core was two less than that in $[Au_{25}(SR)_{18}]^-$. For this reason, the molecular orbitals involved in optical transitions, and thus the observed colors in solution, are different for both.[119] Furthermore, $[Au_{25}(SR)_{18}]^-$ has been shown to exhibit catalytic activity in the oxidation reaction of styrene when the oxidant is $PhI(OAc)_2$, and doping with Pt atoms has been reported by the same group to improve the catalytic activity of the cluster during this reaction.[119] Jiang *et al*. have conducted theoretical studies on $M@Au_{24}(SR)_{18}$ clusters in which the central Au in $Au_{25}(SR)_{18}$ is replaced by various heteroatoms (M).[121] This work predicted that substituting the central Au with 3d transition metals such as Cr, Mn or Fe can endow the cluster with paramagnetism.

3. Protection by Selenolates (SeR)

3.1. $Au_{25}(SeR)_{18}$

It has been reported that gold clusters with increased stability can

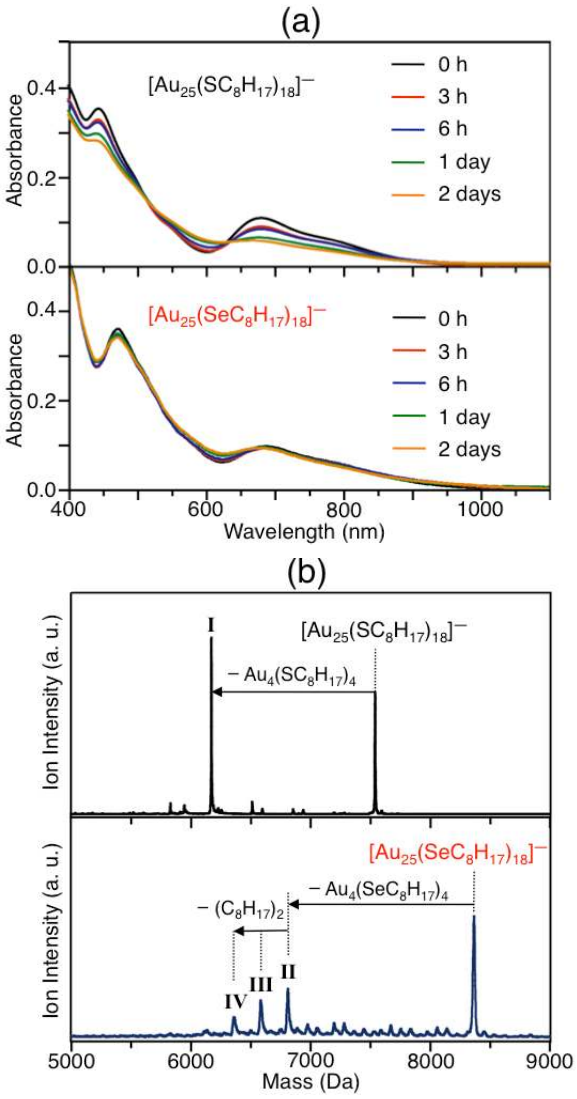

Fig. 12 (a) Variations over time in the absorption spectra of $[Au_{25}(SC_8H_{17})_{18}]^-$ and $[Au_{25}(SeC_8H_{17})_{18}]^-$ in toluene (1×10^{-5} M) at 60 °C. (b) Negative−ion MALDI mass spectra of $[Au_{25}(SC_8H_{17})_{18}]^-$ and $[Au_{25}(SeC_8H_{17})_{18}]^-$ recorded at a high laser fluence. Both spectra were measured at the same laser fluence. **I**−**IV** are assigned to laser fragments (adapted from Ref. 128).

be produced by changing the ligand from thiolate to selenolate (SeR).[91,122] Compared with sulfur (S), the electronegativity and atomic radius of selenium (Se) are closer to those of gold and consequently the Au−SeR bond has more covalent character and has a higher bond energy than Au−SR.[91,123–126] This is expected to make $Au_n(SeR)_m$ more stable than $Au_n(SR)_m$ although, to clarify the correlation between ligand and cluster stability, it is essential to compare the stabilities of clusters with the same quantities of gold atoms and ligands. With the goal of creating a more stable cluster than $Au_n(SR)_m$, we have synthesized $Au_{25}(SeR)_{18}$ which have the same numbers of metal atoms and ligands as the original magic clusters and have investigated their stability.

Synthesis

We prepared the $Au_n(SeR)_m$ clusters using a synthesis method that improves on the approach reported by Li *et al.*[41] We isolated the desired clusters from the mixture of $Au_n(SeR)_m$ clusters based on differences in their solubility in the solvent. Mass and thermogravimetric analyses demonstrated that the product contained only $[Au_{25}(SeC_8H_{17})_{18}]^-$, and thus this product was isolated with high purity (Figure 11(a)).[127]

Structure

Again, it is reasonable to postulate that, given the chemical composition of $[Au_{25}(SeC_8H_{17})_{18}]^-$, it should also have a skeletal structure similar to that of $[Au_{25}(SR)_{18}]^-$. This was strongly supported by the laser dissociation mass spectrum, optical absorption spectrum and powder X-ray diffraction pattern of $[Au_{25}(SeC_8H_{17})_{18}]^-$.[127] In order to improve our understanding of its geometrical structure, we calculated the optimum structure for $[Au_{25}(SeCH_3)_{18}]^-$ and obtained a structure similar to that of $[Au_{25}(SR)_{18}]^-$ (Figure 11(b)).[128] The calculated optical absorption spectrum of $[Au_{25}(SeCH_3)_{18}]^-$ based on this structure closely resembles that of $[Au_{25}(SeC_8H_{17})_{18}]^-$.[128] These results confirm the assumption that the framework structure of the synthesized $[Au_{25}(SeC_8H_{17})_{18}]^-$ is the same as that of $[Au_{25}(SC_8H_{17})_{18}]^-$ and thus the only difference is that they have different ligands.

Stability

To clarify the degree to which changing the ligand affects cluster stability, we first compared the stabilities of $[Au_{25}(SC_8H_{17})_{18}]^-$ and $[Au_{25}(SeC_8H_{17})_{18}]^-$ against degradation in solution and the results indicated that $[Au_{25}(SeC_8H_{17})_{18}]^-$ is more stable than $[Au_{25}(SC_8H_{17})_{18}]^-$ (Figure 12(a)).[128] Au−SeR bonds are more fully covalent and have a higher bond energy than Au−SR and so this enhanced Au–ligand bond energy is considered to increase the stability of the Au_{25} clusters. In a previous study, we found that clusters degrade in solution through detachment of thiolates and/or gold–thiolate oligomers.[51] The higher bond energy of $[Au_{25}(SeC_8H_{17})_{18}]^-$ is considered to suppress this detachment, making it more stable in solution than $[Au_{25}(SC_8H_{17})_{18}]^-$. Based on these results, we conclude that changing the ligand from thiolate to selenolate increases the gold–ligand bond energy in the clusters and thus increases the cluster stability against reactions involving dissociation of these bonds.

We next studied the resistance of solid $[Au_{25}(SC_8H_{17})_{18}]^-$ and $[Au_{25}(SeC_8H_{17})_{18}]^-$ to thermal dissociation. In this work, we employed thermogravimetric analysis (TGA) and estimated the temperature at which the ligands begin to dissociate based on the point where the TGA curve starts to fall. The results demonstrated that the ligands of $[Au_{25}(SeC_8H_{17})_{18}]^-$ begin to dissociate at a lower temperature than those of $[Au_{25}(SC_8H_{17})_{18}]^-$.[128] In this type of dissociation, the alkyl chains begin to separate first.[129] The Se–C bond energy (590.4 kJ/mol) is lower than the S–C bond energy (713.3 kJ/mol) and this lower bond energy is believed to cause the ligands to dissociate at a lower temperature in the case of $[Au_{25}(SeC_8H_{17})_{18}]^-$. We concluded that changing the ligand from thiolate to selenolate reduces the resistance of the ligand to intramolecular dissociation and thus decreases the stability of the clusters with regard to reactions involving this dissociation process. In contrast, in trials involving $[Au_{25}(SC_{12}H_{25})_{18}]^-$ and $[Au_{25}(SeC_{12}H_{25})_{18}]^-$ (Au_{25} clusters protected by ligands with longer alkyl chains), barely any difference was observed between the two during TGA analyses and it was also observed that these clusters with longer alkyl

chains dissociated at higher temperatures. Lengthening the alkyl chain from C_8H_{17} to $C_{12}H_{25}$ increases the intermolecular interactions between ligands and this increase in interactions likely suppresses evaporation of the alkyl groups in both the thiolate and selenolate-based clusters, increasing the evaporation temperature of the alkyl groups in both[130] and giving rise to the minimal difference in these temperatures between $[Au_{25}(SC_{12}H_{25})_{18}]^-$ and $[Au_{25}(SeC_{12}H_{25})_{18}]^-$. These results indicate that if selenolate is used in the ligand, reduced stability due to intramolecular dissociation can be suppressed using a selenolate moiety with a long alkyl chain.

Finally, we investigated the stabilities of $[Au_{25}(SC_8H_{17})_{18}]^-$ and $[Au_{25}(SeC_8H_{17})_{18}]^-$ in response to fragmentation by laser light (N_2 laser; 337 nm), based on measuring the MALDI mass spectra of $[Au_{25}(SC_8H_{17})_{18}]^-$ and $[Au_{25}(SeC_8H_{17})_{18}]^-$ using a high laser fluence. The results indicated that $[Au_{25}(SeC_8H_{17})_{18}]^-$ is more stable against the laser fragmentation of parent ions than $[Au_{25}(SC_8H_{17})_{18}]^-$ (Figure 12(b)).[127] For both clusters, the main dissociation products were assigned as $[Au_{21}(SC_8H_{17})_{14}]^-$ and $[Au_{21}(SeC_8H_{17})_{14}]^-$, which were formed by detachment of the $Au_4(ligand)_4$ moiety from $[Au_{25}(SC_8H_{17})_{18}]^-$ and $[Au_{25}(SeC_8H_{17})_{18}]^-$, respectively.[49] Changing the ligand from thiolate to selenolate increases the bond energy between gold and the ligand and this increase in bond energy suppresses the detachment of the $Au_4(ligand)_4$ group and hence reduces the extent to which fragment ions are generated from $[Au_{25}(SeC_8H_{17})_{18}]^-$ relative to $[Au_{25}(SC_8H_{17})_{18}]^-$.

In summary, the effects on stability of changing the gold cluster ligands from thiolate to selenolate can be summarized as follows: stability is increased during reactions involving dissociation of the gold-ligand bond, while stability decreases in reactions involving intramolecular dissociation of the ligand. However, the latter reduction in stability can be suppressed by incorporating selenolate-based ligands with a long alkyl chain.

These results indicate that Au_{25} clusters protected by selenolates with long alkyl chains have similar stabilities against thermal dissolution and greater stabilities against degradation in solution than Au_{25} clusters protected by thiolates with the same alkyl chain length.

3.2. $Au_{25-n}Cu_n(SeR)_{18}$

As discussed in Section **2.3**, doping $Au_{25}(SR)_{18}$ with an element which has a very different atomic radius from that of Au can significantly reduce the stability of the cluster.[117] To synthesize stable clusters doped with such elements, it is therefore necessary to apply additional modifications to mitigate the deleterious effects of the doping. It was recently reported by our own group,[128] as well as by Meng *et al.*,[122] that the use of selenolate (SeR) groups as ligands allows for the synthesis of a particular form of Au_{25} cluster ($Au_{25}(SeR)_{18}$) that exhibits improved stability compared to $Au_{25}(SR)_{18}$. We expanded on this finding by investigating the Cu doping of $Au_{25}(SeC_8H_{17})_{18}$ clusters. This work succeeded in synthesizing the series of clusters $Au_{25-n}Cu_n(SeC_8H_{17})_{18}$, which we found to be more stable than the analogous S-based clusters $Au_{25-n}Cu_n(SR)_{18}$.

Synthesis and Stability

$Au_{25-n}Cu_n(SeC_8H_{17})_{18}$ (n = 0–9) was produced using the same method applied to the synthesis of $Au_{25}(SeC_8H_{17})_{18}$,[118] with a slight modification. Various characterizations using mass spectrometry demonstrated that the cluster series was synthesized with a high degree of purity via our chosen synthetic approach. Trials to assess the stability of these clusters revealed that the $Au_{25-n}Cu_n(SeC_8H_{17})_{18}$ clusters thus synthesized did not readily degrade in solution and the chemical composition of each cluster was constant under our experimental conditions (Figure 13).[118] The high level of stability exhibited by $Au_{25-n}Cu_n(SeC_8H_{17})_{18}$ is thus superior to that of $Au_{25-n}Cu_n(SC_8H_{17})_{18}$ ($n \geq 1$)[117]. Since the atomic radius of Cu is significantly different from that of Au (1.28 versus 1.44 Å), doping with Cu atoms results in pronounced structural distortion of the cluster, and this effect is considered to be related to the instability of $Au_{25-n}Cu_n(SC_8H_{17})_{18}$ clusters where n = 1–5 (Section **2.3**).[117] Our DFT calculations on $[Au_{25-n}Cu_n(SCH_3)_{18}]^-$ (n = 1–3) imply that the geometric structure of $Au_{25-n}Cu_n(SR)_{18}$ is also significantly distorted when copper is inserted at any cluster site,[118] although the use of selenolates as ligands enhances the strength of the metal–ligand bonds.[128] Although no conclusive results have yet been obtained with regard to the exact Cu atom doping positions, we presume that the increased metal–ligand binding energy is associated with the enhanced stability of $Au_{25-n}Cu_n(SeC_8H_{17})_{18}$ clusters in solution, as in the case of $Au_{25}(SeC_8H_{17})_{18}$.

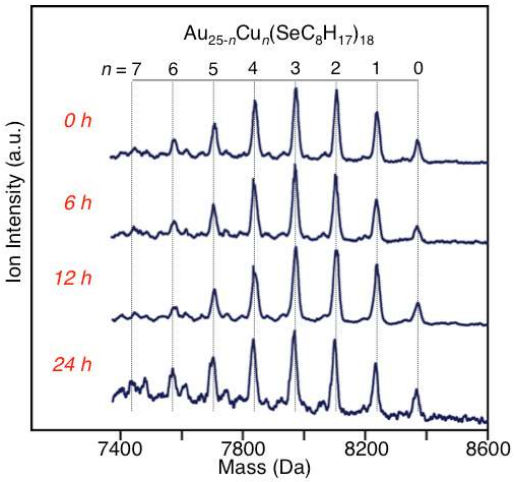

Fig. 13 Time–dependent negative–ion MALDI mass spectra of $Au_{25-n}Cu_n(SeC_8H_{17})_{18}$ in toluene solution (adapted from Ref. 118).

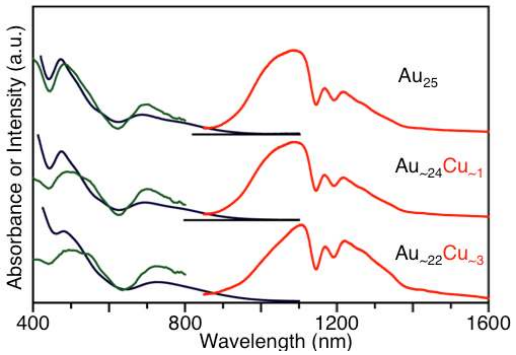

Fig. 14 Absorption (blue), photoluminescence (PL) (red) and excitation (green) spectra of toluene solutions of $Au_{25-n}Cu_n(SeC_8H_{17})_{18}$. PL excitation was at 400 nm. Valleys in the region 1100–1220 nm are due to solvent absorption (adapted from Ref. 118).

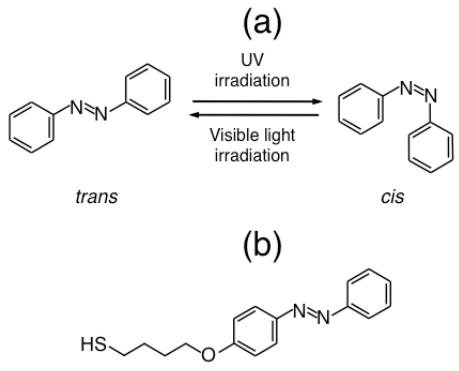

Fig. 15 (a) Illustration of azobenzene photoisomerization. (b) Molecular structure of the azobenzene derivative thiol used in this study.

This work also determined that a greater degree of Cu doping was possible when employing selenolates as ligands as compared to the use of thiolates.[118] When applying thiolate ligands, it is difficult to add more than five Cu atoms per cluster, irrespective of preparative conditions (Figure 9).[117] In contrast, for $Au_{25-n}Cu_n(SeC_8H_{17})_{18}$, the quantity of Cu atoms in the clusters steadily increases as the relative amount of copper salt is increased, such that a [gold salt]:[cupper salt] ratio of 18:7 results in the synthesis of $Au_{16}Cu_9(SeC_8H_{17})_{18}$.[118] These results imply that the use of selenolates as ligands allows for the synthesis of alloy clusters which exhibit a level of stability not achievable with thiolate ligands.

Electronic structure

Optical spectroscopy of a series of $Au_{25-n}Cu_n(SeC_8H_{17})_{18}$ clusters showed that increased levels of Cu doping result in a steady decrease in the HOMO–LUMO gap of the cluster.[118] In the optical absorption spectra of $Au_{25-n}Cu_n(SeC_8H_{17})_{18}$ in toluene solution, the peak attributed to the HOMO–LUMO gap gradually shifts to lower energy levels with increasing amounts of Cu doping. The photoluminescence emission of the clusters also gradually shifts to longer wavelengths with increasing Cu content (Figure 14). These results indicate that Cu doping is an effective means for creating stable clusters with smaller HOMO−LUMO gaps than the original magic $Au_{25}(SeR)_{18}$.

4. Protection by Azobenzene Derivative Thiolates

It has been reported that some of the physical properties of $Au_{25}(SR)_{18}$ change when its ligand structure is modified. For example, the redox potential[100] and photoluminescence quantum yield[77] of $Au_{25}(SR)_{18}$ have been found to depend on the ligand structure. Consequently, combining Au_{25} clusters with thiolates which exhibit reversible structural changes in response to photoirradiation is expected to result in the formation of Au_{25} clusters which change their physical properties reversibly in response to photoirradiation.

Azobenzene is one of the most well-studied photoresponsive molecules. It undergoes isomerisation from its *trans* to its *cis* conformation on UV irradiation and from *cis* to *trans* on visible light irradiation (Figure 15(a)). Thus, combining Au_{25} clusters with azobenzene compounds is expected to result in the formation of clusters whose physical properties change reversibly in response to photoirradiation. We therefore synthesized Au_{25} clusters protected by azobenzene derivative thiolates with the aim of producing photoresponsive Au_{25} clusters.

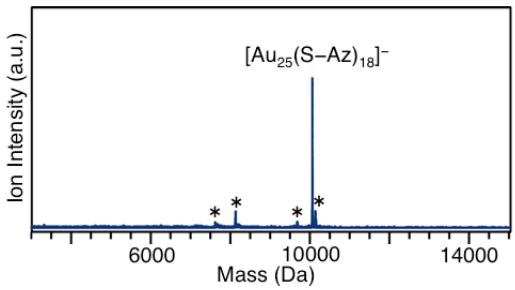

Fig. 16 Negative−ion MALDI mass spectra of $[Au_{25}(S-Az)_{18}]^-$. The asterisks indicate peaks due to fragment ions or phenyl radical adducts (adapted from Ref. 101).

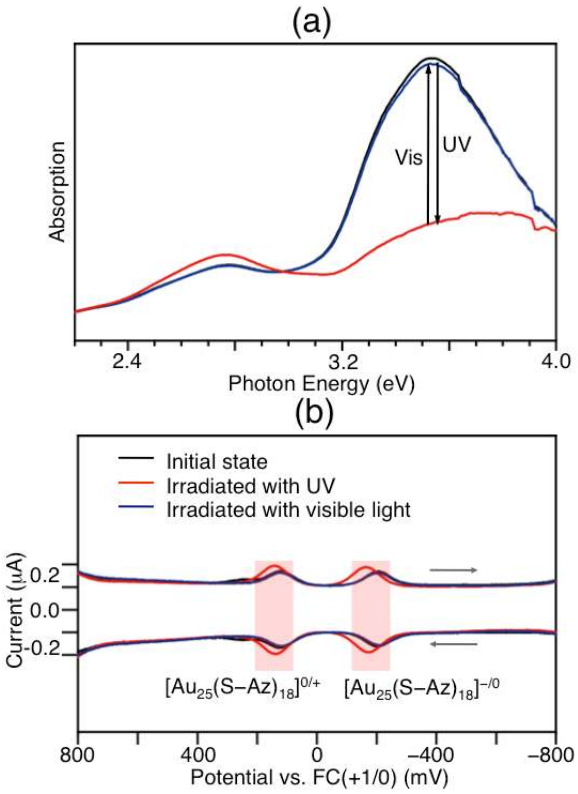

Fig. 17 Photoresponsive behavior of $[Au_{25}(S-Az)_{18}]^-$. (a) Optical absorption spectra of $[Au_{25}(S-Az)_{18}]^-$ toluene solution (5.0×10^{-7} M) in the energy range 2.3–4.0 eV. The visible photostationary state (blue line) overlaps with the initial state (black line). (b) DPV of $[Au_{25}(S-Az)_{18}]^-$. In this experiment, a $[Au_{25}(S-Az)_{18}]^-$ toluene solution (1.0×10^{-5} M) was irradiated by UV and subsequently visible light. After photoirradiation, the photoproducts were evaporated to dryness and were dissolved in a 0.1 M $(C_4H_9)_4NPF_6$ in CH_2Cl_2 solution. DPV was performed at room temperature (adapted from Ref. 101).

Synthesis and Stability

In this study, we used 4–(4–(phenylazo)phenoxy)butyl–1–thiol (Az–SH) as the azobenzene derivative thiolate (Figure 15(b)). This Az–SH was synthesized in our laboratory.[101] $Au_{25}(S-Az)_{18}$ was synthesized using a process similar to that used to make $Au_{25}(SC_2H_4Ph)_{18}$ by Dass *et al.*[104] Mass spectrometry of the product demonstrated that high purity $[Au_{25}(S-Az)_{18}]^-$ protected

by S–Az was synthesized and isolated using this approach (Figure 16). On the basis of various characterizations including optical absorption spectroscopy, laser fragment spectrometry and powder X-ray diffraction, we concluded that $[Au_{25}(S–Az)_{18}]^-$ possesses a similar geometric structure to $[Au_{25}(SC_2H_4Ph)_{18}]^-$.[101]

Isomerization of ligands

The optical absorption spectrum of azobenzene is known to change on isomerization. In the absorption spectrum of the *trans* isomer, a strong peak appears at 3.54 eV (350 nm), which is derived from π–π* absorption, while the spectrum of the *cis* isomer exhibits a less intense peak at 3.54 eV and a peak at 2.75 eV (450 nm) derived from *n*–π* absorption. These spectral changes are reversed when the Az–SH returns to the *trans* conformation. Similar spectral changes were observed repeatedly for isolated $[Au_{25}(S–Az)_{18}]^-$ (Figure 17(a)).[101] These results indicate that azobenzenes reversibly isomerize on photoirradiation even when present in the $[Au_{25}(S–Az)_{18}]^-$ cluster. This finding is in stark contrast to results obtained with two–dimensional self–assembled monolayers (SAMs); it has been reported that isomerization does not occur in two–dimensional SAMs consisting of azobenzene derivative thiolates with a similar structure to the S–Az moiety of Figure 15(b) without the incorporation of spacer molecules.[132] This is because neighboring molecules in two-dimensional SAMs are very close and consequently there is insufficient space for isomerization to occur. The azobenzene–derived thiolates in $[Au_{25}(S–Az)_{18}]^-$, however, are radially distributed around the Au_{13} core and there is thus sufficient space between the ligands for isomerization to take place. This is believed to be responsible for the high photoisomerization efficiency of azobenzenes in $[Au_{25}(S–Az)_{18}]^-$, in contrast to the poor efficiency seen with two–dimensional SAMs.

Photoresponsive behavior of redox potential

The variation in the redox potential of $[Au_{25}(S–Az)_{18}]^-$ due to photoisomerization of the azobenzenes was investigated by differential pulse voltammetry (DPV) measurements. The results clearly demonstrated that the redox potential of $Au_{25}(S–Az)_{18}$ changes reversibly due to photoisomerization of the azobenzenes (Figure 17(b)).[101] In the voltammogram prior to photoirradiation, there are peaks at –206 and 126 mV (Figure 17(b)). By comparison to the voltammogram of $[Au_{25}(SC_2H_4Ph)_{18}]^-$ (Refs. 77, 100, 132), these peaks are attributed to the redox potentials of $[Au_{25}(S–Az)_{18}]^{-1/0}$ and $[Au_{25}(S–Az)_{18}]^{0/+1}$, respectively. In the voltammogram following UV irradiation, these peaks are shifted to higher energies, while the peak positions in the voltammogram after visible light irradiation are similar to those prior to irradiation (Figure 17(b)), indicating that the redox potentials of $[Au_{25}(S–Az)_{18}]^{-1/0}$ and $[Au_{25}(S–Az)_{18}]^{0/+1}$ vary reversibly with photoirradiation. We performed the same studies with $[Au_{25}(SC_2H_4Ph)_{18}]^-$ but did not observe similar peak shifts on photoirradiation[101] which provides further proof that the peak shifts were caused by isomerization of azobenzenes. This variation in the redox potential is considered to be caused by the variation in the intramolecular dipole moment of S–Az due to isomerization of the azobenzenes.[131,134] The variation in the intramolecular dipole moments of ligands is thought to alter the orbital energies of the cluster,[72,132,135,136] causing the redox potential of $[Au_{25}(S–Az)_{18}]^-$ to vary. From these studies, we know that it is possible to produce photoresponsive Au_{25} clusters by incorporating azobenzene derivative thiolates.

5. Summary and Future Directions

In summary, we have attempted to establish methods of functionalizing magic $Au_n(SR)_m$ clusters as a means of creating metal clusters which exhibit stability and unique physical/chemical properties. To this end, we have investigated the effects of heteroatom doping, protection by selenolate ligands and protection by photoresponsive thiolates on these clusters.

With regard to heteroatom doping, Pd, Ag and Cu have all been successfully inserted into magic $Au_n(SR)_m$ clusters. Studies of the resulting clusters showed that: 1) Pd doping improves the stability of the clusters, 2) Ag doping increases the HOMO–LUMO gap in the clusters and 3) Cu doping reduces the HOMO–LUMO gap. These findings can serve as useful design guidelines, since they allow magic $Au_n(SR)_m$ clusters to be endowed with new physical/chemical properties via heteroatom doping. At present, however, clusters doped with Ag or Cu cannot be synthesized with precision at the atomic level. To further our understanding of the effects of doping with these elements on the geometrical and electronic structures of the clusters, it is essential to be able to separate clusters based on the quantity of added dopant atoms. Recent research has demonstrated that HPLC is an extremely effective means of obtaining high-resolution separation of thiolate-protected metal clusters.[33,65,89,119,137,138] The future use of advanced HPLC techniques can thus be expected to allow for high-resolution separation. To date, very little is known about doped clusters, other than information concerning their stability, electronic structures and optical properties. Research into their catalytic activity,[79–82,129] electronic properties[139] and other unique characteristics can be expected to progress in the future.

Studies that have used selenolate as the ligand have found that Au_{25} clusters protected by selenolates are more stable than those protected by thiolates. It is thus expected that stable selenolate-protected Au_{25} clusters will be extensively investigated in the future, just as thiolate-protected Au_{25} clusters are currently being researched. In addition, the same work has demonstrated that the use of selenolates as ligands allows for the synthesis of alloy clusters which exhibit a level of stability not achievable with thiolate ligands. We anticipate that employing selenolate ligands may allow the synthesis of a wide variety of heteroatom-doped Au_{25} clusters.[121,140]

In studies utilizing an azobenzene derivative thiolate as the ligand, it was found that combining Au_{25} clusters with azobenzene compounds result in the formation of Au_{25} clusters which exhibit reversible changes in redox potential in response to photoirradiation. These findings could allow the addition of photoresponsiveness to the other useful physical/chemical properties[131] of magic $Au_n(SR)_m$ clusters.

Acknowledgements

The authors sincerely thank all coworkers whose names appear in the reference section. This work was financially supported by Grants–in–Aid for Scientific Research (No. 20038045, 21685003, 21350018, 25102539, and 25288009) as well as the Next-Generation Supercomputer Project of the Ministry of Education,

Culture, Sports, Science and Technology (MEXT) of Japan. A part of this study was performed in the collaboration program of Institute for Molecular Science. The computation was partly performed at the Research Center for Computational Science, Okazaki, Japan.

Notes and references

[a] *Department of Applied Chemistry, Faculty of Science, Tokyo University of Science, 1-3 Kagurazaka, Shinjuku-ku, Tokyo 162-8601, Japan. Fax: +81-3-5261-4631; Tel: +81-3-5228-9145; E-mail: negishi@rs.kagu.tus.ac.jp*

[b] *Department of Theoretical and Computational Molecular Science, Institute for Molecular Science, Myodaiji, Okazaki, Aichi 444-8585, Japan.*

1 A. W. Castleman, Jr. and K. H. Bowen, Jr., *J. Phys. Chem.*, 1996, **100**, 12911.
2 M. McPartlin, R. Mason and L. Malatesta, *Chem. Commun*., 1969, 334.
3 C. E. Briant, B. R. C. Theobald, J. W. White, L. K. Bell, D. M. P. Mingos and A. J. Welch, *J. Chem. Soc., Chem. Commun.*, 1981, **5**, 201.
4 B. K. Teo, X. Shi and H. Zhang, *J. Am. Chem. Soc*., 1992, **114**, 2743.
5 B. K. Teo and H. Zhang, *Coord. Chem. Rev.*, 1995, **143**, 611.
6 G. Schmid, *Chem. Rev*., 1992, **92**, 1709.
7 K. L. Craighead, A. M. P. Felicissimo, D. A. Krogstad, L. T. J. Nelson and L. H. Pignolet, *Inorg. Chim. Acta*, 1993, **212**, 31.
8 R. Balasubramanian, R. Guo, A. J. Mills and R. W. Murray, *J. Am. Chem. Soc*., 2005, **127**, 8126.
9 Y. Yanagimoto, Y. Negishi, H. Fujihara and T. Tsukuda, *J. Phys. Chem. B*, 2006, **110**, 11611.
10 Y. Liu, H. Tsunoyama, T. Akita and T. Tsukuda, *J. Phys. Chem. C*, 2009, **113**, 13457.
11 T. Inomata and K. Konishi, *Chem. Commun*., 2003, 1282.
12 Y. Shichibu and K. Konishi, *Small*, 2010, **6**, 1216.
13 Y. Kamei, Y. Shichibu and K. Konishi, *Angew. Chem. Int. Ed.*, 2011, **50**, 7442.
14 Y. Shichibu, Y. Kamei and K. Konishi, *Chem. Commun*., 2012, **48**, 7559.
15 Y. Shichibu, K. Suzuki and K. Konishi, *Nanoscale*, 2012, **4**, 4125.
16 W. Kurashige and Y. Negishi, *J. Cluster Science*, 2012, **23**, 365.
17 M. Brust, M. Walker, D. Bethell, D. J. Schiffrin and R. Whyman, *J. Chem. Soc., Chem. Commun.*, 1994, 801.
18 R. L.Whetten, M. N. Shafigullin, J. T. Khoury, T. G. Schaaff, I. Vezmar, M. M. Alvarez and A. Wilkinson, *Acc. Chem. Res.*, 1999, **32**, 397.
19 J. F. Parker, C. A. Fields-Zinna and R. W. Murray, *Acc. Chem. Res.*, 2010, **43**, 1289.
20 T. Tsukuda, *Bull. Chem. Soc. Jpn.*, 2012, **85**, 151.
21 P. Maity, S. Xie, M. Yamauchi and T. Tsukuda, *Nanoscale*, 2012, **4**, 4027.
22 R. Jin, *Nanoscale*, 2010, **2**, 343.
23 H. Qian, M. Zhu, Z. Wu and R. Jin, *Acc. Chem. Res.*, 2012, **45**, 1470.
24 A. Dass, *Nanoscale*, 2012, **4**, 2260.
25 H. Häkkinen, *Nat. Chem.*, 2012, **4**, 443.
26 C. M. Aikens, *J. Phys. Chem. Lett.*, 2011, **2**, 99.
27 A. Sanchez-Castillo, C. Noguez and I. L. Garzón, *J. Am. Chem. Soc*., 2010, **132**, 1504.
28 Y. Pei and X. C. Zeng, *Nanoscale*, 2012, **4**, 4054.
29 D.-e. Jiang, K. Nobusada, W. Luo and R. L. Whetten, *ACS Nano*, 2009, **3**, 2351.
30 D.-e. Jiang and M. Walter, *Nanoscale*, 2012, **4**, 4234.
31 P. D. Jadzinsky, G. Calero, C. J. Ackerson, D. A. Bushnell and R. D. Kornberg, *Science*, 2007, **318**, 430.
32 C. L. Heinecke, T. W. Ni, S. Malola, V. Mäkinen, O. A. Wong, H. Häkkinen and C. J. Ackerson, *J. Am. Chem. Soc.*, 2012, **134**, 13316.
33 I. Dolamic, S. Knoppe, A. Dass and T. Bürgi, *Nature Commun.*, 2012, **3**, 798.
34 H. Yao, *J. Phys. Chem. Lett.*, 2012, **3**, 1701.
35 T. Udayabhaskararao and T. Pradeep, *J. Phys. Chem. Lett.*, 2013, **4**, 1553.
36 Y. Yu, Z. Luo, Y. Yu, J. Y. Lee and J. Xie, *ACS Nano*, 2012, **6**, 7920.
37 S. Antonello, M. Hesari, F. Polo and F. Maran, *Nanoscale*, 2012, **4**, 5333.
38 O. M. Bakr, V. Amendola, C. M. Aikens, W. Wenseleers, R. Li, L. D. Negro, G. C. Schatz and F. Stellacci, *Angew. Chem. Int. Ed.*, 2009, **48**, 5921.
39 S. Kumar, M. D. Bolan and T. P. Bigioni, *J. Am. Chem. Soc.*, 2010, **132**, 13141.
40 J. Guo, S. Kumar, M. Bolan, A. Desireddy, T. P. Bigioni and W. P. Griffith, *Anal. Chem.*, 2012, **84**, 5304.
41 Y. Li, O. Zaluzhna, B. Xu, Y. Gao, J. M. Modest and Y. Y. J. Tong, *J. Am. Chem. Soc.*, 2011, **133**, 2092.
42 K. Kwak and D. Lee, *J. Phys. Chem. Lett.*, 2012, **3**, 2476.
43 H. Kouchi, H. Kawasaki and R. Arakawa, *Anal. Methods*, 2012, **4**, 3600.
44 R. L. Whetten, J. T. Khoury, M. M. Alvarez, S. Murthy, I. Vezmar, Z. L. Wang, P. W. Stephens, C. L. Cleveland, W. D. Luedtke and U. Landman, *Adv. Mater.*, 1996, **8**, 428.
45 T. G. Schaaff and R. L. Whetten, *J. Phys. Chem. B*, 2000, **104**, 2630.
46 R. C. Price and R. L. Whetten, *J. Am. Chem. Soc.*, 2005, **127**, 13750.
47 R. L. Donkers, D. Lee and R. W. Murray, *Langmuir*, 2004, **20**, 1945.
48 J. B. Tracy, G. Kalyuzhny, M. C. Crowe, R. Balasubramanian, J.-P. Choi and R. W. Murray, *J. Am. Chem. Soc.*, 2007, **129**, 6706.
49 A. Dass, A. Stevenson, G. R. Dubay, J. B. Tracy and R. W. Murray, *J. Am. Chem. Soc.*, 2008, **130**, 5940.
50 Y. Negishi, Y. Takasugi, S. Sato, H. Yao, K. Kimura and T. Tsukuda, *J. Am. Chem. Soc.*, 2004, **126**, 6518.
51 Y. Negishi, K. Nobusada and T. Tsukuda, *J. Am. Chem. Soc.*, 2005, **127**, 5261.
52 H. Tsunoyama, Y. Negishi and T. Tsukuda, *J. Am. Chem. Soc.*, 2006, **128**, 6036.
53 Y. Shichibu, Y. Negishi, H. Tsunoyama, M. Kanehara, T. Teranishi and T. Tsukuda, *Small*, 2007, **3**, 835.
54 Y. Negishi, N. K. Chaki, Y. Shichibu, R. L. Whetten and T. Tsukuda, *J. Am. Chem. Soc.*, 2007, **129**, 11322.
55 N. K. Chaki, Y. Negishi, H. Tsunoyama, Y. Shichibu and T. Tsukuda, *J. Am. Chem. Soc.*, 2008, **130**, 8608.
56 C. A. Fields-Zinna, R. Sardar, C. A. Beasley and R. W. Murray, *J. Am. Chem. Soc.*, 2009, **131**, 16266.
57 H. Qian and R. Jin, *Nano Lett.*, 2009, **9**, 4083.
58 M. Zhu, H. Qian and R. Jin, *J. Am. Chem. Soc.*, 2009, **131**, 7220.
59 H. Qian, Y. Zhu and R. Jin, *J. Am. Chem. Soc.*, 2010, **132**, 4583.
60 C. Zeng, H. Qian, T. Li, G. Li, N. L. Rosi, B. Yoon, R. N. Barnett, R. L. Whetten, U. Landman and R. Jin, *Angew. Chem. Int. Ed.*, 2012, **51**, 13114.
61 H. Qian, Y. Zhu and R. Jin, *Proc. Natl. Acad. Sci. U.S.A.*, 2012, **109**, 696.
62 A. Dass, *J. Am. Chem. Soc.*, 2009, **131**, 11666.
63 A. Dass, *J. Am. Chem. Soc.*, 2011, **133**, 19259.
64 P. R. Nimmala, B. Yoon, R. L. Whetten, U. Landman and A. Dass, *J. Phys. Chem. A*, 2013, **117**, 504.
65 Y. Negishi, C. Sakamoto, T. Ohyama and T. Tsukuda, *J. Phys. Chem. Lett.*, 2012, **3**, 1624.
66 S. Knoppe, A. C. Dharmaratne, E. Schreiner, A. Dass and T. Bürgi, *J. Am. Chem. Soc.*, 2010, **132**, 16783.
67 M. W. Heaven, A. Dass, P. S. White, K. M. Holt and R. W. Murray, *J. Am. Chem. Soc.*, 2008, **130**, 3754.
68 M. Zhu, C. M. Aikens, F. J. Hollander, G. C. Schatz and R. Jin, *J. Am. Chem. Soc.*, 2008, **130**, 5883.
69 M. Zhu, W. T. Eckenhoff, T. Pintauer and R. Jin, *J. Phys. Chem. C*, 2008, **112**, 14221.
70 H. Qian, W. T. Eckenhoff, Y. Zhu, T. Pintauer and R. Jin, *J. Am. Chem. Soc.*, 2010, **132**, 8280.
71 J. Akola, M. Walter, R. L. Whetten, H. Häkkinen and H. Grönbeck, *J. Am. Chem. Soc.*, 2008, **130**, 3756.
72 C. M. Aikens, *J. Phys. Chem. Lett.*, 2010, **1**, 2594.
73 O. Lopez-Acevedo, H. Tsunoyama, T. Tsukuda, H. Häkkinen and C. M. Aikens, *J. Am. Chem. Soc.*, 2010, **132**, 8210.
74 D.-e. Jiang, *Nanoscale*, 2013, DOI:10.1039/C3NR34192E.
75 S. Link, A. Beeby, S. FitzGerald, M. A. El-Sayed, T. G. Schaaff and R. L. Whetten, *J. Phys. Chem. B*, 2002, **106**, 3410.
76 D. Lee, R. L. Donkers, G. Wang, A. S. Harper and R. W. Murray, *J.*

Am. Chem. Soc., 2004, **126**, 6193.
77 Z. Wu and R. Jin, *Nano Lett.*, 2010, **10**, 2568.
78 S. Knoppe, I. Dolamic, A. Dass and T. Bürgi, *Angew. Chem. Int. Ed.*, 2012, **51**, 7589.
79 Y. Zhu, H. Qian, B. A. Drake and R. Jin, *Angew. Chem. Int. Ed.*, 2010, **49**, 1295.
80 Y. Zhu, H. Qian and R. Jin, *J. Mater. Chem.*, 2011, **21**, 6793.
81 X. Nie, H. Qian, Q. Ge, H. Xu and R. Jin, *ACS Nano*, 2012, **6**, 6014.
82 G. Li, H. Qian and R. Jin, *Nanoscale*, 2012, **4**, 6714.
83 R. Guo, Y. Song, G. Wang and R. W. Murray, *J. Am. Chem. Soc.*, 2005, **127**, 2752.
84 J. B. Tracy, M. C. Crowe, J. F. Parker, O. Hampe, C. A. Fields-Zinna, A. Dass and R. W. Murray, *J. Am. Chem. Soc.*, 2007, **129**, 16209.
85 C. A. Fields-Zinna, J. F. Parker and R. W. Murray, *J. Am. Chem. Soc.*, 2010, **132**, 17193.
86 V. R. Jupally, R. Kota, E. V. Dornshuld, D. L. Mattern, G. S. Tschumper, D.-e. Jiang and A. Dass, *J. Am. Chem. Soc.*, 2011, **133**, 20258.
87 E. S. Shibu, M. A. H. Muhammed, T. Tsukuda and T. Pradeep, *J. Phys. Chem. C*, 2008, **112**, 12168.
88 Y. Niihori, W. Kurashige, M. Matsuzaki and Y. Negishi, *Nanoscale*, 2013, **5**, 508.
89 Y. Niihori, M. Matsuzaki, T. Pradeep and Y. Negishi, *J. Am. Chem. Soc.*, 2013, **135**, 4946.
90 M. Akutsu, K. Koyasu, J. Atobe, N. Hosoya, K. Miyajima, M. Mitsui and A. Nakajima, *J. Phys. Chem. A*, 2006, **110**, 12073.
91 C. K. Yee, A. Ulman, J. D. Ruiz, A. Parikh, H. White and M. Rafailovich, *Langmuir*, 2003, **19**, 9450.
92 Y. Negishi, H. Tsunoyama, Y. Yanagimoto and T. Tsukuda, *Chem. Lett.*, 2005, **34**, 1638.
93 C. A. Fields-Zinna, M. C. Crowe, A. Dass, J. E. F. Weaver and R. W. Murray, *Langmuir*, 2009, **25**, 7704.
94 D.-e. Jiang and S. Dai, *Inorg. Chem.*, 2009, **48**, 2720.
95 K. A. Kacprzak, L. Lehtovaara, J. Akola, O. Lopez-Acevedo, and H. Häkkinen, *Phys. Chem. Chem. Phys.*, 2009, **11**, 7123.
96 M. Walter and M. Moseler, *J. Phys. Chem. C*, 2009, **113**, 15834.
97 We used both $C_{12}H_{25}SH$ and PhC_2H_4SH as the ligands in all studies. We successfully isolated the target cluster $Au_{24}Pd(SR)_{18}$ only when we employing $C_{12}H_{25}SH$, while $Au_{36}Pd_2(SR)_{24}$ was isolated only when we used PhC_2H_4SH.
98 Y. Negishi, W. Kurashige, Y. Niihori, T. Iwasa and K. Nobusada, *Phys. Chem. Chem. Phys.*, 2010, **12**, 6219.
99 M. Laupp and J. Strähle, *Angew. Chem. Int. Ed. Engel*, 1994, **33**, 207.
100 D. Lee, R. L. Donkers, G. Wang, A. S. Harper and R. W. Murray, *J. Am. Chem. Soc.*, 2004, **126**, 6193.
101 Y. Negishi, U. Kamimura, M. Ide and M. Hirayama, *Nanoscale*, 2012, **4**, 4263.
102 A. Dass, K. Holt, J. F. Parker, S. W. Feldberg and R. W. Murray, *J. Phys. Chem. C*, 2008, **112**, 20276.
103 Y. Song and R. W. Murray, *J. Am. Chem. Soc.*, 2002, **124**, 7096.
104 A. C. Dharmaratne, T. Krick and A. Dass, *J. Am. Chem. Soc.*, 2009, **131**, 13604.
105 Y. Negishi, K. Igarashi, K. Munakata, W. Ohgake and K. Nobusada, *Chem. Commun.*, 2012, **48**, 660.
106 H. Qian, E. Barry, Y. Zhu and R. Jin, *Acta Phys. –Chim. Sin.*, 2011, **27**, 513.
107 ESI mass spectrometry implied that $Au_{36}Pd_2(SC_2H_4Ph)_{24}$ was synthesized as the dianionic species $[Au_{36}Pd_2(SCH_3)_{24}]^{2-}$.
108 Y. Negishi, T. Iwai and M. Ide, *Chem. Commun.*, 2010, **46,** 4713.
109 E. Gottlieb, H. Qian and R. Jin, *Chem. Eur. J.*, 2013,**19**, 4238.
110 E. B. Guidez, V. Mäkinen, H. Häkkinen and C. M. Aikens, *J. Phys. Chem. C*, 2012, **116**, 20617.
111 D. R. Kauffman, D. Alfonso, C. Matranga, H. Qian and R. Jin, *J. Phys. Chem. C*, 2013, **117**, 7914.
112 M. Walter, J. Akola, O. Lopez-Acevedo, P. D. Jadzinsky, G. Calero, C. J. Ackerson, R. L. Whetten, H. Grönbeck and H. Häkkinen, *Proc. Natl. Acad. Sci. U.S.A.*, 2008, **105**, 9157.
113 C. M. Aikens, *J. Phys. Chem. C*, 2008, **112**, 19797.
114 C. Kumara and A. Dass, *Nanoscale*, 2012, **4**, 4084.
115 C. Kumara and A. Dass, *Nanoscale*, 2011, **3**, 3064.
116 S. Malola and H. Häkkinen, *J. Phys. Chem. Lett.*, 2011, **2**, 2316.
117 Y. Negishi, K. Munakata, W. Ohgake and K. Nobusada, *J. Phys. Chem. Lett.*, 2012, **3**, 2209.
118 W. Kurashige, K. Munakata, K. Nobusada and Y. Negishi, *Chem. Commun.*, 2013, **49**, 5447.
119 H. Qian, D.-e. Jiang, G. Li, C. Gayathri, A. Das, R. R. Gil and R. Jin, *J. Am. Chem. Soc.*, 2012, **134**, 16159.
120 S. L. Christensen, M. A. MacDonald, A. Chatt, P. Zhang, H. Qian and R. Jin, *J. Phys. Chem. C*, 2012, **116**, 26932.
121 D.-e. Jiang and R. L. Whetten, *Phys. Rev. B*, 2009, **80**, 115402.
122 X. Meng, Q. Xu, S. Wang and M. Zhu, *Nanoscale*, 2012, **4**, 4161.
123 F. K. Huang, R. C. Horton, Jr., D. C. Myles and R. L. Garrell, *Langmuir*, 1998, **14**, 4802.
124 Y. Sato and F. Mizutani, *Phys. Chem. Chem. Phys.*, 2004, **6**, 1328.
125 T. Weidner, A. Shaporenko, J. Müller, M. Höltig, A. Terfort and M. Zharnikov, *J. Phys. Chem. C*, 2007, **111**, 11627.
126 E. de la Llave and D. A. Scherlis, *Langmuir*, 2010, **26**, 173.
127 Y. Negishi, W. Kurashige and U. Kamimura, *Langmuir*, 2011, **27**, 12289.
128 W. Kurashige, M. Yamaguchi, K. Nobusada and Y. Negishi, *J. Phys. Chem. Lett.*, 2012, **3**, 2649.
129 S. Xie, H. Tsunoyama, W. Kurashige, Y. Negishi and T. Tsukuda, *ACS Catal.*, 2012, **2**, 1519.
130 H. Qian and R. Jin, *Chem. Mater.*, 2011, **23**, 2209.
131 M. Suda, N. Kameyama, M. Suzuki, N. Kawamura and Y. Einaga, *Angew. Chem.*, 2008, **120**, 166.
132 S. D. Evans, S. R. Johnson, H. Ringsdorf, L. M. Williams and H. Wolf, *Langmuir*, 1998, **14**, 6436.
133 R. Guo and R. W. Murray, *J. Am. Chem. Soc.*, 2005, **127**, 12140.
134 M. Suda, N. Kameyama, A. Ikegami and Y. Einaga, *J. Am. Chem. Soc.*, 2009, **131**, 865.
135 A. H. Holm, M. Ceccato, R. L. Donkers, L. Fabris, G. Pace and F. Maran, *Langmuir*, 2006, **22**, 10584.
136 M. S. Devadas, K. Kwak, J.-W. Park, J.-H. Choi, C.-H. Jun, E. Sinn, G. Ramakrishna and D. Lee, *J. Phys. Chem. Lett.*, 2010, **1**, 1497.
137 R. L. Wolfe and R. W. Murray, *Anal. Chem.*, 2006, **78**, 1167.
138 S. Xie, M. C. Paau, Y. Zhang, S. Shuang, W. Chan and M. M. F. Choi, *Nanoscale*, 2012, **4**, 5325.
139 H. Zhang, Y. Yasutake, Y. Shichibu, T. Teranishi and Y. Majima, *Phys. Rev. B*, 2005, **72**, 205441.
140 J. U. Reveles, P. A. Clayborne, A. C. Reber, S. N. Khanna, K. Pradhan, P. Sen and M. R. Pederson, *Nat. Chem.*, 2009, **1**, 310.